Interaction between two laser-induced cavitation bubbles in a quasi-two-dimensional geometry

PEDRO A. QUINTO-SU AND CLAUS-DIETER OHL†

School of Physical and Mathematical Sciences, Division of Physics and Applied Physics,
Nanyang Technological University, 21 Nanyang Link, Singapore 637371

We report on experimental and numerical studies of pairs of cavitation bubbles growing and collapsing close to each other in a narrow gap. The bubbles are generated with a pulsed and focused laser in a liquid-filled gap of 15 µm height; during their lifetime which is shorter than 14 µs they expand to a maximum radius of up to $R_{max} = 38$ µm. Their motion is recorded with high-speed photography at up to 500 000 frames s^{-1}. The separation at which equally sized bubbles are created, d, is varied from $d = 46$–140 µm which results into a non-dimensional stand-off distance, $\gamma = d/(2R_{max})$, from 0.65 to 2. For large separation the bubbles shrink almost radially symmetric; for smaller separation the bubbles repulse each other during expansion and during collapse move towards each other. At closer distances we find a flattening of the proximal bubbles walls. Interestingly, due to the short lifetime of the bubbles ($\leqslant 14$ µs), the radial and centroidal motion can be modelled successfully with a two-dimensional potential flow ansatz, i.e. neglecting viscosity. We derive the equations for arbitrary configurations of two-dimensional bubbles. The good agreement between model and experiments supports that the fluid dynamics is essentially a potential flow for the experimental conditions of this study. The interaction force (secondary Bjerknes force) is long ranged dropping off only with $1/d$ as compared to previously studied three-dimensional geometries where the force is proportional to $1/d^2$.

1. Introduction

The attraction and repulsion of oscillating objects in an inviscid fluid has been studied for more than a century (Basset 1887). In general, attraction between objects occurs when they oscillate in phase and repulsion for out-of-phase oscillations (Lamb 1932). Of particular interest is the case of a single bubble positioned at a distance $d/2$ away from the boundary. For a rigid boundary this is identical to two equally sized bubbles being d apart and oscillating in phase. The bubble is attracted towards the boundary. Vice versa for a pressure release boundary the bubble is repelled.

The mutual forces generated between oscillating objects have been named secondary Bjerknes forces after C. A. Bjerknes and his son V. Bjerknes (Bjerknes 1906, 1915; Leighton 1994); in contrast the primary Bjerknes force is due to the direct interaction between an oscillating body and a sound field. Numerous theoretical and experimental studies (for example Crum 1975; Luther, Mettin & Lauterborn 2000; Harkin, Kaper & Nadim 2001; Doinikov 2004; Illinskii, Hamilton & Zabotskaya 2007) have confirmed this general picture and detailed the models to account for viscous and close range

† Email address for correspondence: cdohl@ntu.edu.sg

effects. On the experimental side bubbles can be brought into oscillatory motion with a resonant sound field or by transiently releasing energy. In most of the previous works, oscillating bubbles were studied using axisymmetry or three-dimensional geometry. Interestingly, only recently the two-dimensional potential flow has re-gained broader interest. Wang (2004) and Crowdy, Surana & Yick (2007) used conformal mapping to solve the flow of two circular disks and planar stirrers, respectively, and Nair & Kanso (2007) used a Lagrangian approach to describe the coupling of one oscillating and one rigid object. To our knowledge, very few experiments have been reported demonstrating the interaction of two-dimensional bubbles: Zwaan *et al.* (2007) demonstrated that a single bubble oscillating in a narrow gap can be described for short times with a two-dimensional potential flow and the classical work by Dear, Field & Walton (1988) on the collapse of two-dimensional cavities. Yet, the authors are unaware of previous works comparing two-dimensional oscillating and interacting objects with a two-dimensional model. However, two-dimensional models have been successfully used to describe the collapse of cylindrical voids in liquids and soft sand (Oguz & Prosperetti 1993; Lohse *et al.* 2004; Bergmann *et al.* 2006). The bubbles reported here are created with focused laser light, shaped using a spatial light modulator (SLM). This newly developed technique (Quinto-Su, Venugopalan & Ohl 2008) allows for arbitrary bubble configurations, in particular it allows to modify the geometry and size of the bubbles by changing the pattern of the computer-controlled SLM. In this way it is easy to tune the interaction between the bubbles going from a weakly to a strongly interacting regime.

This work is organized as follows: First we describe the experimental setup used to create the bubbles using a digital hologram. Then we present experimental results for bubble expanding and collapsing at different separations in a narrow gap. In §4 we show the applicability of the two-dimensional model for the experimental configurations, in particular we first derive the equations of motion for the radial and the translational motion and compare them with the experimental data.

2. Experimental set-up

In this section we describe the experimental set-up used to create the bubble pairs using a single laser pulse to create a couple of foci at the focal plane of a microscope objective. The bubbles are the result of the explosive vaporization of the liquid following stress confinement (see references in Quinto-Su *et al.* 2008). The experimental set-up (Quinto-Su *et al.* 2008) is shown in figure 1(*a*) and consists of a laser, optics for beam shaping, a microscope and a high-speed camera. The laser to generate the bubbles is a frequency doubled Nd:YAG (Orion, New Wave Research, Fremont, CA) with a 6 ns pulse duration. The beam shaping is done with a half-wave plate to rotate the plane of polarization and a telescope consisting of lenses L_1 and L_2 to expand it. Then the beam is reflected from a spatial light modulator (SLM) that changes its phase. A digital hologram is projected onto the SLM, so that the spatial profile of the reflected laser pulse after being focused is related to the hologram through a Fourier transformation. To remove the undiffracted zeroth order a lens phase is added to the hologram. A third lens (L_3) images the SLM onto the back aperture of the microscope objective ($20\times$, NA = 0.75) of the inverted microscope (Olympus IX-71, Singapore). With the appropriate hologram a pair of foci is created at the focal plane of the microscope objective. The sample is illuminated with the microscope lamp from the top and the bubble dynamics is recorded with a high-speed camera (Photron SA1.1, Bucks, UK) at 450 000–500 000 frames s^{-1} (f.p.s.). Motion
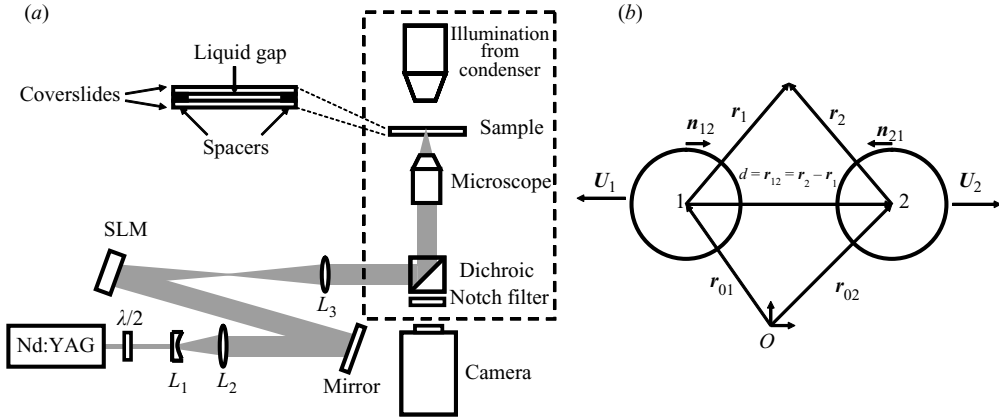
FIGURE 1. (*a*) Experimental setup; the phase of the laser pulse is altered by the SLM, which is imaged onto the back aperture of the microscope objective. A pair of foci is created in the focal plane of the microscope objective which is located inside the liquid gap (15 μm in height). (*b*) Bubble geometry. The positions of the bubbles (radii R_1 and R_2) have their centres at r_{01} and r_{02} and translate with velocities U_1 and U_2.

blurring is mostly avoided by limiting the exposure time for each frame to 300 ns. The two-dimensional narrow gap is made with two spacers with a height of 15 μm which are sandwiched between a couple of microscope coverslips (#1, 130–170 μm thickness). The gap is filled with magenta ink (MAXTEC universal ink refill, Kowloon, HongKong) to obtain stress confinement and still transmit sufficient light to record the events at the short exposure times. We measured the density and the viscosity of the water-based ink. The density is $\rho = 1046 \pm 1 \text{ kg m}^{-3}$ and the kinematic viscosity at 25 °C is $\nu = (1.98 \pm 0.4) \times 10^{-6} \text{ m}^2 \text{ s}^{-1}$. In the experiment the intense illumination will considerably heat up the light-absorbing ink, still below the boiling point. Thus we expect a decrease of the kinematic viscosity and roughly estimate the magnitude by a factor of 0.5 which is found for water when heated from 25 °C to 50 °C. Additionally, we added some 2 μm polystyrene particles to the ink to visualize the flow field.

2.1. *Geometry of the bubble pair*

Figure 1(*b*) shows the configuration of the bubble pair with radii R_1 and R_2. The vectors to the centre of each bubble are r_{01} and r_{02} and their translational velocities are $U_1 = \dot{r}_{01}$ and U_2. The distance between them is $d = r_{12}$. Further we make use of the unit vectors $n_{12} = (r_2 - r_1)/|r_2 - r_1|$ and $n_{21} = -n_{12}$. Also, we can describe the positions relative to the centre of each bubble using the vectors r_1 and r_2, respectively.

3. Experimental results

In this section we first show the dynamics of equally sized bubble pairs created at three different distances spanning the range from weak to strong interactions. To specify the interaction we make use of the non-dimensional standoff distance $\gamma = d/(2R_{max})$ which for the experiments shown varies from $\gamma = 0.65$ to $\gamma = 2$. In addition, we also present one case showing two bubbles of unequal sizes. The next four figures (figures 2–5) are arranged in the following way: figures 2(*a*)–5(*a*) show the high-speed recordings and figures 2(*b,c*)–5(*b,c*) the bubble radii and distances as a function of time, respectively. For figures 2(*a*)–5(*a*), the circles (o) depict the position of the laser foci where the bubbles are created and the asterisks (*) their

(*a*)

(*b*)

(*c*)
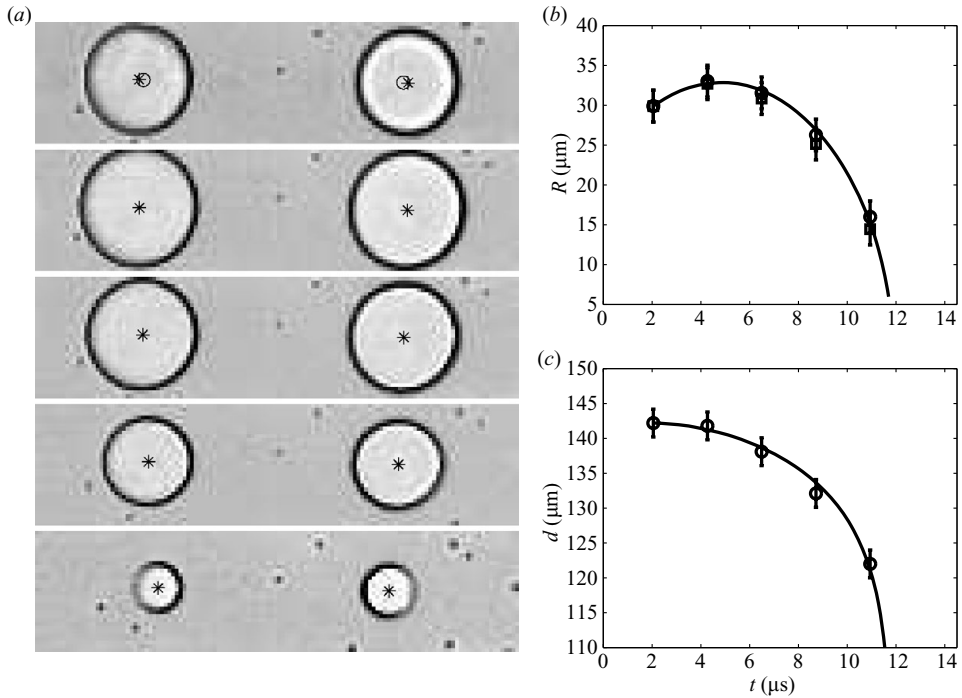
Figure 2. (*a*) Two equally sized bubbles created at a distance of 137.5 μm. The framing speed is 450 000 f.p.s. and the frame width is 256 μm. (*b*) Symbols showing the measured radii as a function of time for each bubble. (*c*) Distance between the bubbles' centres as a function of time. The solid lines in (*b*) and (*c*) are solutions of the two-dimensional potential model.

centre of mass. Time zero is defined when the bubble is created, i.e. the laser pulse arrives at the liquid. Each data point in figures 2(*b*,*c*)–5(*b*,*c*) corresponds to one experimental frame from figures 2(*a*)–5(*a*). The solid lines on each plot are a fit to a two-dimensional potential flow model (see §4).

3.1. *Weak interaction,* $\gamma = 2$

Figure 2 shows two bubbles created at a distance of 140 μm (circles in first frame). Their maximum radii R_{max} are about 35 μm. The bubbles' centres have moved 5 μm away from each other during the time of bubble generation and the first recorded frame. During the shrinkage or collapse of the bubbles attraction is found. They move approximately 20 μm towards each other. In all but the last frame the bubbles remain cylindrical. In the last frame the outward edges of the bubbles appear blurred, this is due to the formation of fast counter-propagating jets (Naudé & Ellis 1961).

3.2. *Intermediate interaction,* $\gamma = 1.3$

In figure 3 the bubbles are created 93 μm apart. Here, we see again an initial displacement of the bubbles' centres during the expansion which is slightly larger than that for the previous case. During collapse the total change in distance between the bubbles, d, is now 35 μm, thus 75 % higher than before. Also, we observe a slight deformation of the proximal bubble walls. Again, in the last frame the distal bubble walls of the shrinking bubbles are blurred due to the jet flows.
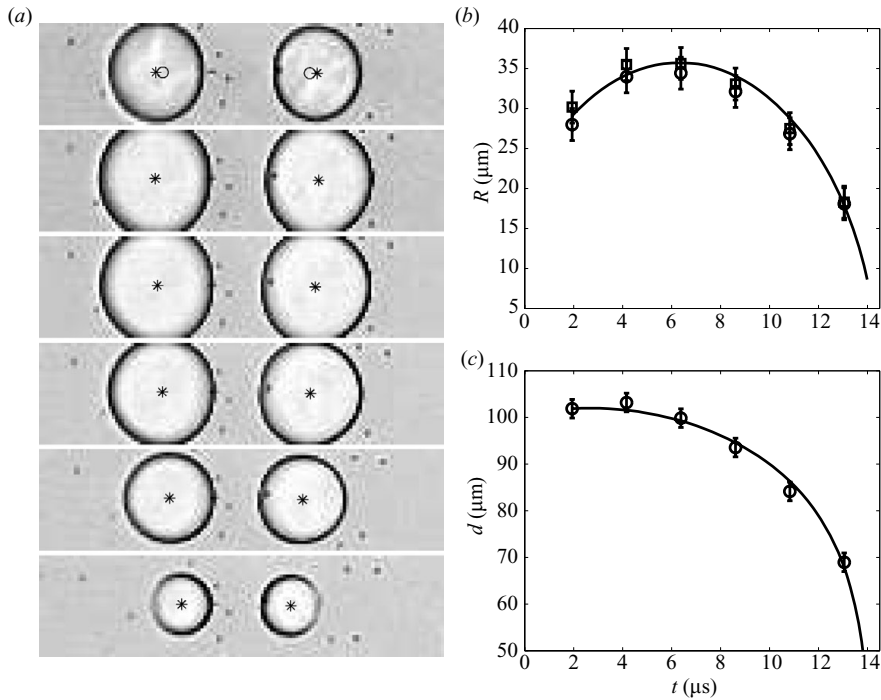
FIGURE 3. (*a*) Two equally sized bubbles created at a distance of 93 μm. The framing speed is 450 000 f.p.s. and the frame width is 256 μm. (*b*) Symbols showing the measured radii as a function of time for each bubble. (*c*) Distance between the bubbles' centres as a function of time. The solid lines in (*b*) and (*c*) are solutions of the two-dimensional potential model.

3.3. *Strong interaction,* $\gamma = 0.65$

Figure 4 shows a bubble pair created at a distance of 46 μm. The bubbles repel during the first 4 μs. Although the distal bubble walls remain cylindrical the proximal walls flatten severely forming a straight channel in between. The thickness of this channel decreases, yet coalescence does not occur for this initial separation. Equivalent radii of these deformed bubbles are obtained by measuring the area; the centre of each bubble is taken as their centre of mass. The total reduction in the distance between the bubbles is more than 40 μm, almost covering the entire initial separation between the bubbles. In the last frame the two counter-propagating jets become vaguely visible.

3.4. *Bubbles with unequal sizes*

Figure 5 shows two bubbles of different size; the digital hologram is adjusted so that one of the spots created at the focus of the microscope objective receives less laser energy, thus leading to a smaller bubble. The initial distance between them is 70 μm. Only four data points are given for the distance because of the early collapse of the smaller bubble. During the lifetime of the smaller bubble the larger bubble moves considerably less than the smaller one. The smaller bubble collapses first and jets towards the larger bubble which is starting to collapse in the fourth frame of figure 5(*a*). It is worth mentioning the pointed shape of the large bubble towards the left in the last frame.
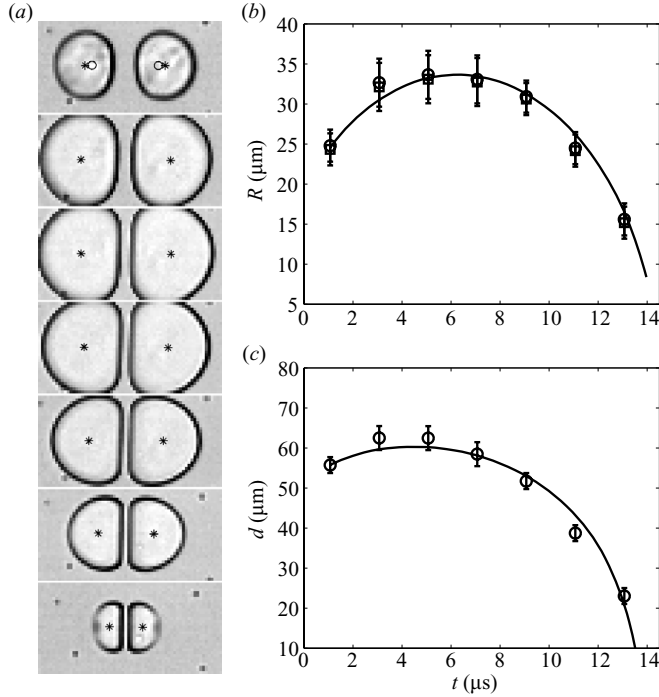
FIGURE 4. (*a*) Two equally sized bubbles created at a distance of 46 μm. The framing speed is 500 000 f.p.s. and the frame width is 128 μm. (*b*) Symbols showing the measured radii as a function of time for each bubble. (*c*) Distance between the bubbles' centres as a function of time. The solid lines in (*b*) and (*c*) are solutions of the two-dimensional potential model.

4. Two-dimensional potential flow model

We now model the flow in the centre of the channel to derive equations for the radial and translational dynamics of arbitrary bubble configurations. The time needed for vorticity to diffuse from the boundaries to the centre of the channel is approximated by the time for the displacement thickness to reach to the channel's centre $\tau = y^2/(1.72^2 \nu)$, where ν is the viscosity and y is half the height of the liquid gap (Batchelor 1967). Thus, for these very brief times, $t < \tau$, the flow in the channel's centre is not affected by the no-slip boundary conditions as it is decoupled from the boundary layers; this allows to decompose the flow in a flow at the channel's centre and a flow at the boundaries. The latter is a viscosity-dominated boundary layer flow whereas the central flow is basically irrotational. Thus the flow in the centre of the channel can be modelled for sufficiently short times with a velocity potential $\phi = \phi(r, t < \tau)$ which satisfies the Laplace equation $\nabla^2 \phi = 0$. Inserting the estimated viscosity of the liquid $\nu \approx 1 \times 10^{-6}$ m^2 s^{-1} (see §2) and the channel height of $y = 7.5$ μm we obtain $\tau < 19$ μs. The online supplementary material presents the dynamics for bubbles of different sizes, there we see that for larger bubbles with a lifetime τ of more than 18 μs, it is not possible to ignore the boundary layer. The consequence is as expected, large bubbles will be affected by viscosity and cannot be modelled with the potential model derived below.

Viscous effects can also be introduced through the viscous stresses at the bubble interface. This however, can be safely ignored for low-viscosity liquids used in this experiment for most of the bubble dynamics, in particular for the inertia-dominated
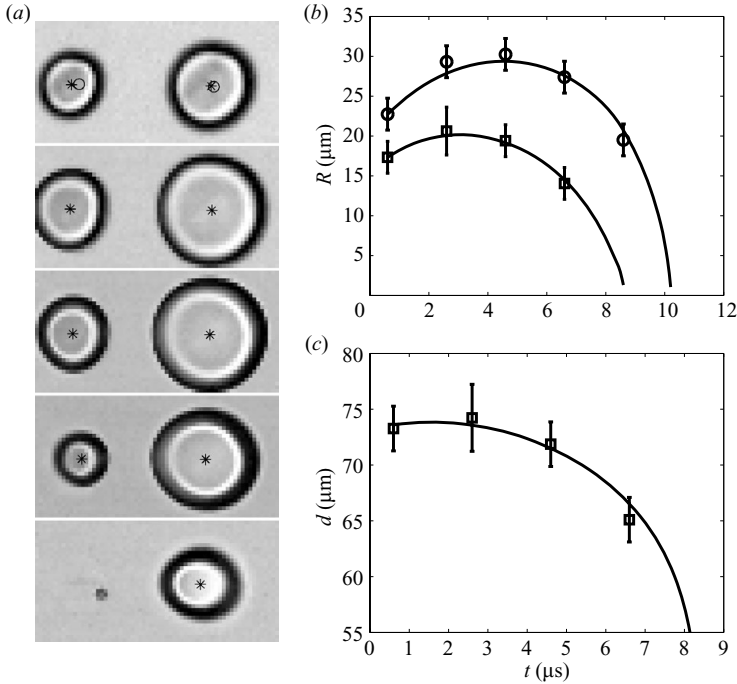
FIGURE 5. (*a*) Two bubbles created at a distance of 70 μm. The framing speed is 500 000 f.p.s. and the frame width is 128 μm. The last frame depicts on the left the remains from smaller bubble after its first collapse. This data is excluded from the graphs. (*b*) Symbols showing the measured radii as a function of time for each bubble. (*c*) Distance between the bubbles' centres as a function of time. The solid lines in (*b*) and (*c*) are solutions of the two-dimensional potential model.

expansion and collapse phase studied here (Hilgenfeldt *et al.* 1998). Further we want to mention that due to the high Reynolds numbers the advection terms in the Navier–Stokes equation cannot be ignored, thus a Hele-Shaw modelling approach is ruled out (Batchelor 1967).

4.1. *Velocity potential*

The derivation of a solution of the Laplace equation is analogues to Lagrangian formalism presented by Illinskii *et al.* (2007). There, it has been applied to derive equations of motion for arbitrary configurations of N oscillating spherical bubbles. Following their method now in two dimensions we obtain $2N$ coupled ordinary differential equations for the bubble radius and its position.

First considering a single bubble labelled i: at the surface of this bubble the fluid velocity is equal to the radial velocity added to the bubble's translational velocity; thus the boundary condition (BC) for the single bubble potential ϕ_{0i} is

$$\left.\frac{\partial\phi_{0i}}{\partial r_i}\right|_{r_i=R_i} = \dot{R}_i + \boldsymbol{U_i},\cdot\boldsymbol{n_i}, \qquad (4.1)$$

where $\dot{R}_i$ is the radial velocity, $\boldsymbol{U_i}$ the translational velocity and $\boldsymbol{n_i}$ is the surface normal. Following the ansatz (Luther *et al.* 2000; Illinskii *et al.* 2007) the potential can be split into a monopole and dipole terms $\phi(\boldsymbol{r_i})_{0i} = a\log(r_i/R_\infty) + b/r_i$. Here, R_∞ is a normalization constant for the argument of the logarithmic term and is later

identified as the distance at which the velocity drops to zero, i.e. to limit the kinetic energy of the system (Lohse *et al.* 2004; Zwaan *et al.* 2007). We obtain the functions *a* and *b* by implementing BC (4.1), thus the single bubble potential reads

$$\phi_{0i}(\boldsymbol{r}_i) = R_i \dot{R}_i \log\left(\frac{r_i}{R_\infty}\right) - \frac{R_i^2 \boldsymbol{U}_i \cdot \boldsymbol{n}_i}{r_i}. \tag{4.2}$$

To construct the potential for N interacting bubbles we sum over all potentials (Illinskii *et al.* 2007) $\phi(\boldsymbol{r}_i) = \sum_i \phi_{0i}(\boldsymbol{r}_i) = \phi_{0i}(\boldsymbol{r}_i) + \sum_{i \neq k} \phi_{0k}(\boldsymbol{r}_k)$ and write it as a Taylor series of first order

$$\phi(\boldsymbol{r}_i) = \phi_{0i}(\boldsymbol{r}_i) + \sum_{k \neq i} \phi_{0k}(\boldsymbol{r}_{ki} + \boldsymbol{r}_i) = \phi_{0i}(\boldsymbol{r}_i) + \sum_{k \neq i} [\phi_{0k}(\boldsymbol{r}_{ki}) + \boldsymbol{c}_{ki} \cdot \boldsymbol{r}_i + \cdots], \tag{4.3}$$

where $\boldsymbol{r}_{ki} = \boldsymbol{r}_{0i} - \boldsymbol{r}_{0k}$, and

$$\boldsymbol{c}_{ki} = \left(\frac{\partial \phi_{0k}(\boldsymbol{r}_k)}{\partial r_k}\right)\bigg|_{r_k = r_{ki}} = \frac{R_k \dot{R}_k}{r_{ki}} \boldsymbol{n}_{ki} - \frac{R_k^2}{r_{ki}^2}[\boldsymbol{U}_k - 2(\boldsymbol{U}_k \cdot \boldsymbol{n}_{ki})\boldsymbol{n}_{ki}] \tag{4.4}$$

To satisfy BC (4.1) corrections are needed to cancel the terms $\boldsymbol{c}_{ki} \cdot \boldsymbol{n}_i$ in (4.3). This can be achieved by adding $\phi_{1i}(\boldsymbol{r}_i) = (R_i^2/r_i)\boldsymbol{c}_{ki} \cdot \boldsymbol{n}_i$ to the right-hand side of (4.3). The potential now reads $\phi(\boldsymbol{r}_i) = \phi_{0i}(\boldsymbol{r}_i) + \phi_{1i}(\boldsymbol{r}_i) + \sum_{k \neq i}[\phi_{0k}(\boldsymbol{r}_{ki}) + \boldsymbol{c}_{ki} \cdot \boldsymbol{r}_i + \phi_{1k}(\boldsymbol{r}_{ki})]$.

The kinetic energy of the liquid K can be expressed as $K = (\rho/2)\int_S |\nabla\phi|^2 dS = -(\rho/2)\sum_i \int_{l_i} \phi(\partial\phi/\partial r_i)dl_i$, where S is the surface over whole liquid domain, and l_i are the contours of the cylindrical bubbles. Implementing BC (4.1) the kinetic energy becomes $K = -(\rho/2)\sum_i \int_{l_i} (\dot{R}_i + \boldsymbol{U}_i \cdot \boldsymbol{n}_i)\phi dl_i$. To calculate the kinetic energy, the potential on the surface of the ith bubble has to be evaluated. For the Lagrangian we need additionally the potential energy V in two dimensions, thus $V = \int p dS$. Here, we neglect the gas and vapour pressure inside the bubble and also surface tension. Then, the potential energy simplifies to $V = \sum_i \pi R_i^2 p_0$, where p_0 is the ambient pressure.

4.2. *Lagrangian equation*

Combining the kinetic energy K and the potential energy V we obtain the Lagrangian

$$L = \sum_i \frac{1}{2}\pi R_i^2 \rho \boldsymbol{U}_i^2 - \sum_{i,k,i \neq k} R_i R_k \dot{R}_i \dot{R}_k \pi\rho \log\left(\frac{R_i r_{ik}}{R_\infty^2}\right)$$

$$+ \sum_{i,k,i \neq k} \frac{R_i R_k}{r_{ik}}\left[R_i \dot{R}_k(\boldsymbol{U}_i \cdot \boldsymbol{n}_{ik}) + R_k \dot{R}_i(\boldsymbol{U}_k \cdot \boldsymbol{n}_{ki})\right] - \sum_i \pi R_i^2 p_0. \tag{4.5}$$

The equations of motion for the system are derived from the Lagrangian equations; thus for the radial dynamics $d(\partial L/\partial \dot{R}_i)/dt = \partial L/\partial R_i$, and $d(\partial L/\partial \dot{r}_{0i})/dt = \partial L/\partial r_{0i}$ for the translational dynamics.

4.3. *Equations of motion for bubble radii*

From the Lagrangian we obtain the following equation:

$$\left(\ddot{R}_i R_i + \dot{R}_i^2\right)\log\left(\frac{R_i}{R_\infty}\right) + \frac{\dot{R}_i^2}{2} = \frac{p}{\rho} - \frac{\boldsymbol{U}_i^2}{2} - \sum_{k \neq i}(\ddot{R}_k R_k + \dot{R}_k^2)\log\left(\frac{r_{ik}}{R_\infty}\right). \tag{4.6}$$

This is a two-dimensional Rayleigh equation (Rayleigh 1917) for a single bubble in two dimensions with additional pressure terms on the right-hand side. The second term on the right-hand side of (4.6) $\boldsymbol{U}_i^2$ is a dynamic pressure reduction of the
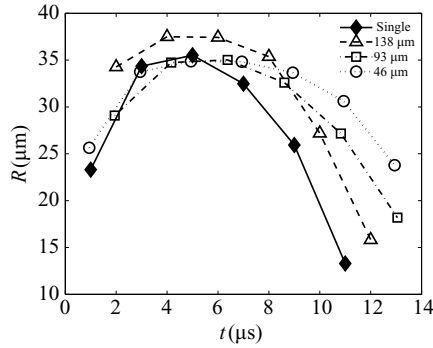
FIGURE 6. Comparing the radial dynamics of a single bubble (black diamonds) with those of similar interacting bubbles. For clarity, we removed the error bars which have a size of $\pm 2\,\mu$m. The lines joining the points are placed to guide the eye.

moving bubble and the last on the right-hand side of (4.6) is the imposed pressure from neighbouring bubbles. This term couples the radial motion with the translational motion. Please note that for the derivation of (4.6) terms of the order $O(r_{ik}^{-1})$ are neglected as those are much smaller than the dominant $\log(r_{ik}/R_\infty)$.

4.4. *Equations of motion for bubble position*

The equation of motion for the bubble position is

$$\ddot{\boldsymbol{r}}_{0i} = -\frac{2\dot{R}_i U_i}{R_i} + \sum_{k \neq i} \frac{\boldsymbol{n}_{ki}\left(R_k \ddot{R}_k + \dot{R}_k^2\right)}{r_{ki}}. \tag{4.7}$$

The second term of (4.7) is due to the interaction with all other bubbles $k \neq i$, thus it is related to the secondary Bjerknes force. It scales as $1/r_{ik}$ which is in contrast to the three-dimensional case where it depends on the inverse square of the distance.

The model assumes zero pressure inside the bubble; it ignores thermodynamics or mass transfer inside the bubble. This assumption does surely not hold during the early bubble expansion which is driven by superheated liquid explosively expanding into a vaporous cavity. Also during this stage the bubble cannot be described with as two-dimensional cavity. We limit our model to the later stages of expansion where the bubble has cooled and is sufficiently flat to be considered two-dimensional. Thus, we model the bubble expansion with an already cylindrical bubble and an initial radial velocity $\dot{R}$.

5. Discussion

5.1. *Bubble lifetime*

The experiments in §3 reveal that the radial and translational dynamics are greatly altered by the mutual interaction. To unravel this further we directly compare the single bubble dynamics with bubble pairs of similar radius. This is experimentally achieved by using the same hologram and by blocking one of the foci, thus keeping the laser energy per bubble unchanged.

This comparison is shown in figure 6 for different separations. All bubbles reach a maximum radius of about $35\,\mu$m, the single bubble collapses first (filled diamonds), about $11\,\mu$s after creation which is significantly shorter than all bubble pairs. The lifetime of the pairs increases with decreasing stand-off distance.

5.2. *Comparison with experiments*

After presenting the experimental results for bubble pairs in figures 2–5 we now want to compare them with the model derived in §4. The initial conditions for the translational and radial dynamics are needed to integrate the equations of motion because we ignore the early stage of the bubble formation. The initial values for bubble radius and bubble position are obtained from the experimental data. The initial conditions for the bubble wall and the translational velocities, $\dot{R}_1$ and $\dot{d} = 2\dot{r}_{01}$, are obtained by least-square fitting of (4.6) and (4.7) to the experimental data. Also a unique value for R_∞ for our experimental configuration has to be obtained. Therefore, we fitted the measured radius time curves from single bubbles, e.g. the one presented in figure 6, to a two-dimensional Rayleigh equation $(R\ddot{R} + \dot{R}^2)\log(R/R_\infty) + \dot{R}^2/2 = (p_0/\rho)$. The best fit is $R_\infty = 546\,\mu\text{m}$ and is used for all curves presented in this work.

The model describes the observed dynamics for all bubble pairs studied. In particular, even the dynamics of the strongly deformed bubbles (strong interaction with $\gamma = 0.65$, see figure 4) is nicely captured within the measurement errors. Here, instead of the bubble radius, an equivalent radius is used still giving good agreement with the cylindrical model. It is interesting to note (see figures 2–4) that the reduction of the distance d during the collapse increases as the bubbles are created closer which is consistent with the secondary Bjerknes force.

Bremond *et al.* (2006*b*) used hydrophobic microcavities etched in silicon wafers to study arbitrary bubble configurations and compare the dynamics with the three-dimensional coupled Rayleigh equations. They obtained very good agreement with this simple ansatz, although for close range interaction a boundary integral method was applied (Bremond *et al.* 2006*a*). In a two-dimensional geometry bubble interaction has a longer range $(1/d)$ as compared to the three-dimensional Bjerknes force $(1/d^2)$.

6. Conclusions

We recorded the dynamics of two bubbles created at different distances in an essentially two-dimensional geometry. By varying the distance at which the bubbles were created we were able to 'tune' the interaction between the bubbles from a weakly to a strongly interacting regime. A two-dimensional flow potential model is derived from the Lagrangian of the coupled bubble system. The model accounts for radial and translational dynamics for arbitrary configurations of cylindrical bubbles. The radial dynamics is a Rayleigh equation with additional terms due to the mutual interactions. The model is in very good agreement with the experimental results. Future studies will involve specific bubble configurations of interest in microfluidics, in particular for object manipulation, microrheology and mixing applications.

REFERENCES

Basset, A. B. 1887 On the motion of two spheres in a liquid. *Proc. Lond. Math. Soc.* **18**, 369–378.
Batchelor, G. K. 1967 *An Introduction to Fluid Dynamics*. Cambridge University Press.

Bergmann, R., van der Meer, D., Stijnman, M., Sandtke, M., Prosperetti, A. & Lohse, D. 2006 Giant bubble pinch-off. *Phys. Rev. Lett.* **96**, 154505.

Bjerknes, C. A. 1915 *Hydrodynamische Fernkraft*. Engelmann.

Bjerknes, V. F. K. 1906 *Fields of Force*. Columbia University Press.

Bremond, N., Arora, M., Dammer, S. M. & Lohse, D. 2006a Interaction of cavitation bubbles on a wall. *Phys. Fluids* **18**, 121505.

Bremond, N., Arora, M., Ohl, C. D. & Lohse, D. 2006b Controlled multibubble surface cavitation. *Phys. Rev. Lett.* **18**, 121505.

Crowdy, D. G., Surana, A. & Yick, K.-Y. 2007 The irrotational flow generated by two planar stirrers in inviscid fluid. *Phys. Fluids* **19**, 018103.

Crum, L. A. 1975 Bjerknes forces on bubbles in a stationary sound field. *J. Acoust. Soc. Am.* **57**, 1363–1370.

Dear, J. P., Field, J. E. & Walton, A. J. 1988 Gas compression and jet formation in cavities collapsed by a shock wave. *Nature* **332**, 505–508.

Doinikov, A. 2004 Mathematical model for collective bubble dynamics in strong ultrasound fields. *J. Acoust. Soc. Am.* **116**, 821–827.

Harkin, A., Kaper, T. J. & Nadim, A. 2001 Coupled pulsation and translation of two gas bubbles in a liquid. *J. Fluid Mech.* **445**, 377–411.

Hilgenfeldt, S., Brenner, M. P., Grossmann, S. & Lohse, D. 1998 Analysis of Rayleigh–Plesset dynamics for sonoluminescing bubbles. *J. Fluid Mech.* **365**, 171–204.

Illinskii, Y. A., Hamilton, M. F. & Zabolotskaya, E. A. 2007 Bubble interaction dynamics in Lagrangian and Hamiltonian mechanics. *J. Acoust. Soc. Am.* **121**, 786–795.

Lamb, H. 1932 *Hydrodynamics*, 6th edition. Cambridge University Press.

Leighton, T. G. 1994 *The Acoustic Bubble*. Academic Press.

Lohse, D., Bergmann, R., Mikkelsen, R., Zeilstra, C., van der Meer, D., Versluis, M., van der Weele, K., van der Hoef, M. & Kuipers, H. 2004 Impact on soft sand: void collapse and jet formation. *Phys. Rev. Lett.* **93**, 198003.

Luther, S., Mettin, R. & Lauterborn, W. 2000 Modeling acoustic cavitation by a Lagrangian approach. In *Nonlinear Acoustics at the Turn of the Milenium, ISNA 15th International Symposium on Nonlinear Acoustics* (ed. W. Lauterborn & T. Kurz), International Symposia on Nonlinear Acoustics, vol. 524, pp. 351–354. AIP.

Nair, S. & Kanso, E. 2007 Hydrodynamically-coupled rigid bodies. *J. Fluid Mech.* **592**, 393–411.

Naudé, C. F. & Ellis, A. T. 1961 On the mechanism of cavitation damage by non hemispherical cavities collapsing in contact with a solid boundary. *Trans. ASME D.: J. Basic Engng* **83**, 648–656.

Oguz, H. N. & Prosperetti, A. 1993 Dynamics of bubble growth and detachment from a needle. *J. Fluid Mech.* **257**, 111–145.

Quinto-Su, P. A., Venugopalan, V. & Ohl, C. D. 2008 Generation of laser-induced cavitation bubbles with a digital hologram. *Opt. Exp.* **16**, 18964–18969.

Rayleigh, L. 1917 On the pressure developed in a liquid during the collapse of a spherical cavity. *Phil. Mag.* **34**, 94–98.

Wang, Q. X. 2004 Interaction of two circular cylinders in inviscid fluid. *Phys. Fluids* **16**, 4412–4425.

Zwaan, E., Gac, S. Le, Tsuji, K. & Ohl, C. D. 2007 Controlled cavitation in microfluidic systems. *Phys. Rev. Lett.* **98**, 254501.